Electronic Supplementary Information

Highly efficient Mn-Mn dimer activated phosphor for high-power near-infrared LED application

Xiaoshuang Li[†#], Tianpeng Liu[†#], Kang Zhang[†], Zhiyu Hu[†], Hongxiang An[†], Shuwei Deng[†], Youchao Kong[‡*] and Bo Wang[†*]

[†]School of Applied Physics and Materials, Wuyi University, Jiangmen, Guangdong 529020, P.R. China

[‡]Department of Physics and Electronic Engineering, Yancheng Teachers University, Yancheng 224002, P. R. China

[*]**Corresponding Authors:**

yb87816@connect.um.edu.mo

wangbo312@mails.ucas.ac.cn

EXPERIMENTAL SECTION

Materials and synthesis. New phosphor samples with nominal composition of $LaZn_{1-x}Al_{11}O_{19}$: xMn^{2+} (x = 0 - 0.4) were prepared via solid-state reaction method at 1600℃ for 4 hours under 85% N_2+15% H_2 reductive atmosphere by using the starting reagents: La_2O_3, ZnO, Al_2O_3, SiO_2 and $MnCO_3$ (A.R.) powders.

The PiG sample was prepared by co-sintering $LaZn_{1-x}Al_{11}O_{19}$: xMn^{2+} phosphor particles and the TeO_2-B_2O_3-ZnO-Na_2O low-melting glass via a two-step melt-quenching method. Precursor glasses were prepared by a conventional melting-quenching method. The reagent grade chemicals were mixed thoroughly and melted in a platinum crucible at 750 ℃ for 0.5 h in ambient atmosphere. Then, the melt was poured into a cold copper mold and then cooled to room temperature. The prepared glass was milled to powders using a ball grinder, and then mixed with the $La(Zn,Mn)Al_{11}O_{19}$ phosphors thoroughly and sintered in a platinum crucible at 540 ℃ for 20 min in ambient atmosphere.[1-2] As a proof-of-concept experiment, the remote-type NIR-LED was constructed by encapsulating a stacking PiG plate on the commercial blue chip (InGaN~ 450 nm). The PiG color converter was horizontally fastened on the blue chip, with opaque silica gel coated around the edge to prevent leakage of blue light.

Characterization. The powder X-ray diffraction (PXRD) patterns of the as-obtained samples were collected on a X' Pert PRO diffractometer (Cu Kα radiation, λ = 1.5406 Å) at 298 K. The microstructure was analyzed using a scanning electron microscope (SEM, JSM-6700F). The X-ray photoelectron spectroscopy (XPS, Thermo

fisher Scientific K-Alpha) was conducted to identify the chemical states of the elements in the sample. A FLS-980 fluorescence spectrophotometer (Xe 900, 450 W arc lamps) was employed to obtain the photoluminescence (PL), photoluminescence excitation (PLE), and decay curve spectra. An absolute photoluminescence quantum yield measurement system (Hamamatsu, Quantaurus-QY plus C13534-31) was adopted to test the quantum efficiency. The photoelectric performance of the obtained w-LED device was measured in an integrating sphere of 50 cm diameter, which was connected to a CCD detector with an optical fiber (ATA 100, Everfine).

Computational methods. Utilizing density functional theory (DFT) as implemented in the Vienna *ab-initio* simulation package code,[3] we investigate the electronic structures of title compound. We used projector augmented wave (PAW) method[4] for the ionic cores and the generalized gradient approximation (GGA) for the exchange-correlation potential, in which the Perdew-Burke-Ernzerhof (PBE) type[5] exchange-correlation was adopted. The reciprocal space was sampled with 0.03 $Å^{-1}$ spacing in the Monkhorst-Pack scheme for structure optimization, while denser k-point grids with 0.01 $Å^{-1}$ spacing were adopted for properties calculation. We used a mesh cutoff energy of 400 eV to determine the self-consistent charge density. All geometries are relaxed until the Hellmann-Feynman force on atoms is less than 0.01 eV/Å and the total energy change is less than 1.0×10^{-5} eV. The calculation models were built from the crystal structure.

[1] D.Y. Huang, Z.Y. Liu, B. Wang, H.L. Che, M. Zou, Q.G. Zeng, H.Z. Lian, J. Lin, Highly efficient yellow-orange emission and superior thermal stability of

$Ba_2YAl_3Si_2O_{12}:Ce^{3+}$ for high-power solid lighting. *J. Am. Ceram. Soc*. 2021, 104, 524-534.

[2] Z.K. Chen, B. Wang, X.S. Li, D.Y. Huang, H.Y. Sun, Q.G. Zeng, Chromaticity-tunable and thermal stable phosphor-in-glass inorganic color converter for high power warm w-LEDs. *Mater.* 2018, 11, 1792.

[3] G. Kresse, J. Furthmüller, Efficient iterative schemes for ab-initio total-energy calculations using a plane-wave basis set. *Phys. Rev. B* 1996**,** 54, 11169-11186.

[4] G. Kresse, D. Joubert, From ultrasoft pseudopotentials to the projector augmented-wave method. *Phys. Rev. B* 1999, 59, 1758-1775.

[5] P.E. Blöchl, Projector augmented-wave method. *Phys. Rev. B* 1994**,** 50, 17953-17979.

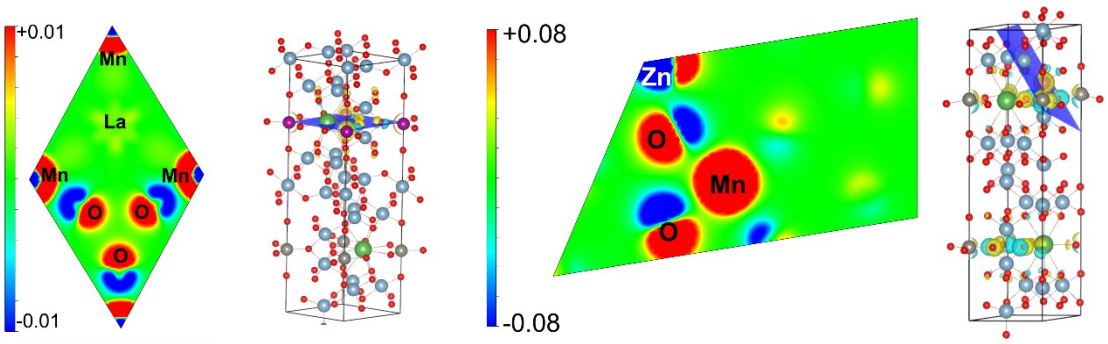

Figure S1. 2D plot of deformation charge when one Mn atom replace the Al or Zn site.

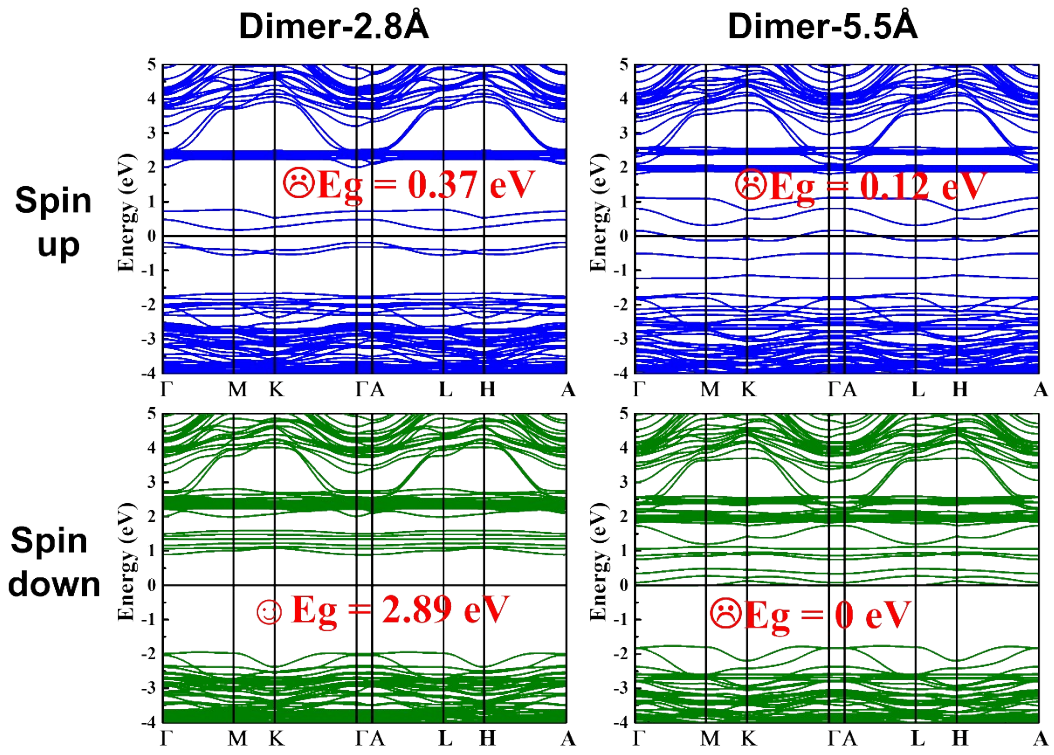

Figure S2. Spin-polarized band structure of D1 and D3 models. The Fermi energy is set to 0 eV.

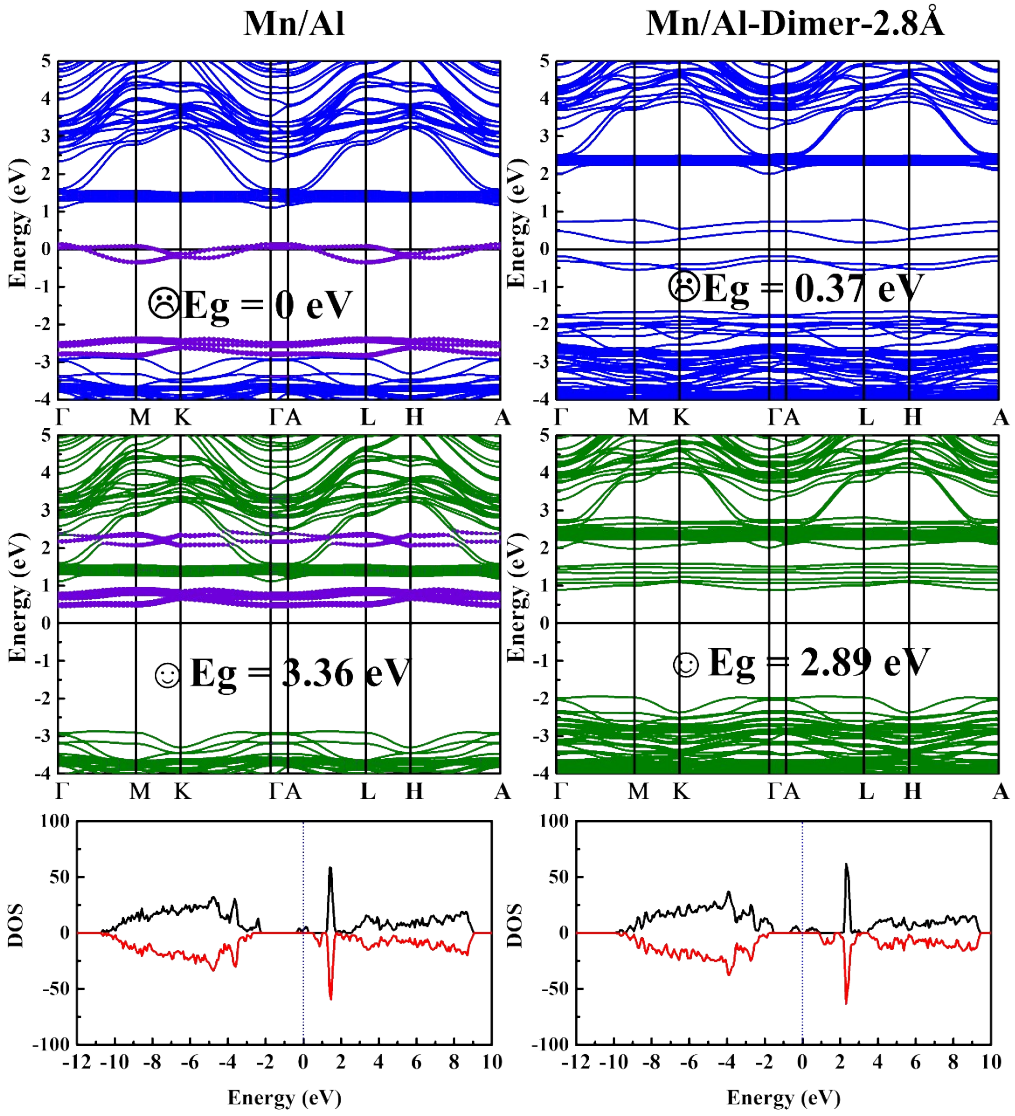

Figure S3. Spin-polarized band structure and DOS of Mn single and dimer doped models. The Fermi energy is set to 0 eV.

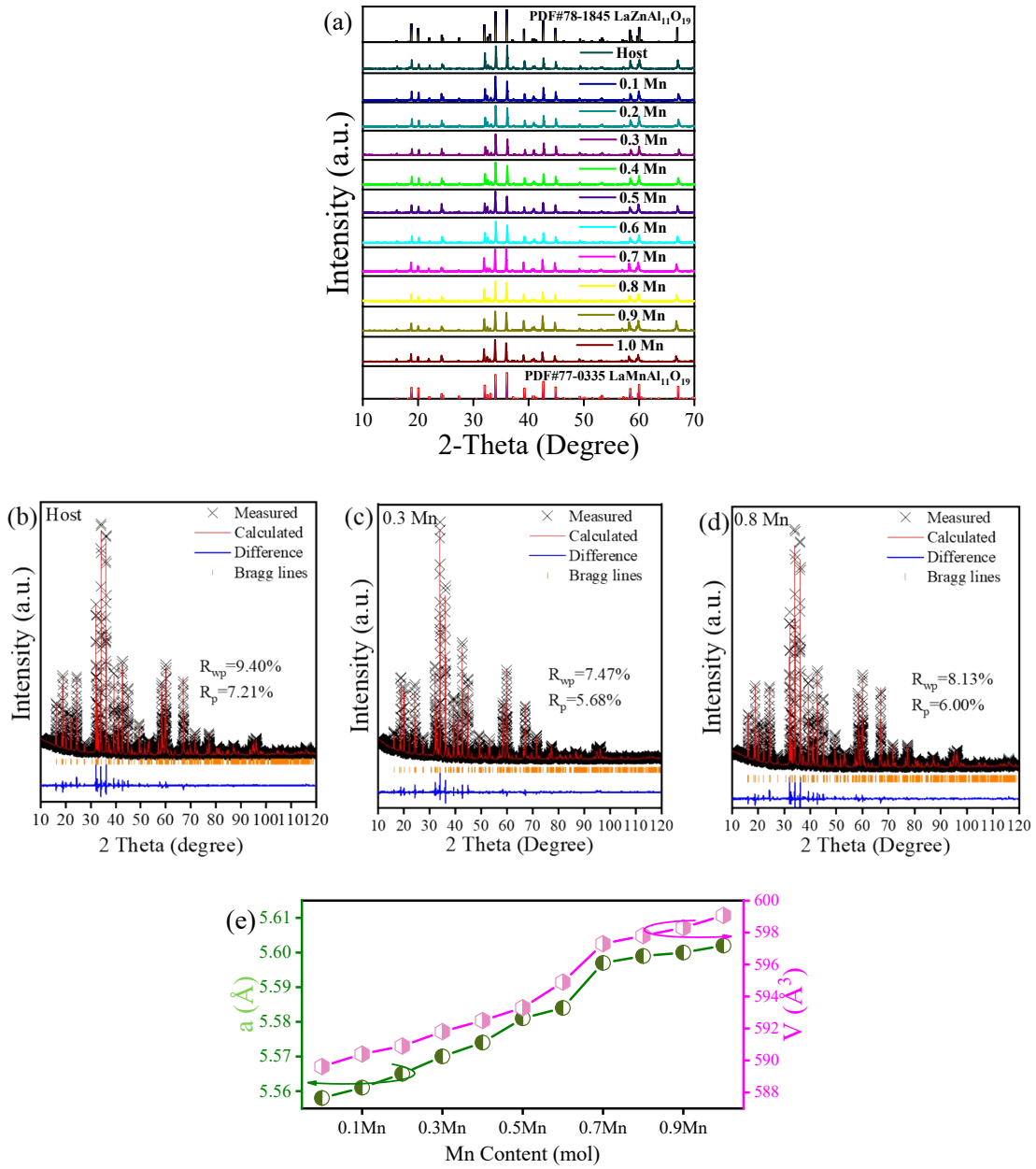

Figure S4. (a) XRD patterns of $La(Zn_{1-x}Mn_x)Al_{11}O_{19}$ (x = 0-1) and standard cards PDF# No. 78-1845 ($LaZnAl_{11}O_{19}$) and No. 77-0335 ($LaMnAl_{11}O_{19}$). (b-d) The representative Rietveld refinements of samples with x=0, 0.3 and 0.8, the red lines, the black crosses and the yellow short lines represent the calculated patterns, experimental patterns and the Bragg reflection positions, respectively. (e) the lattice parameters of $La(Zn_{1-x}Mn_x)Al_{11}O_{19}$ (x = 0-1).

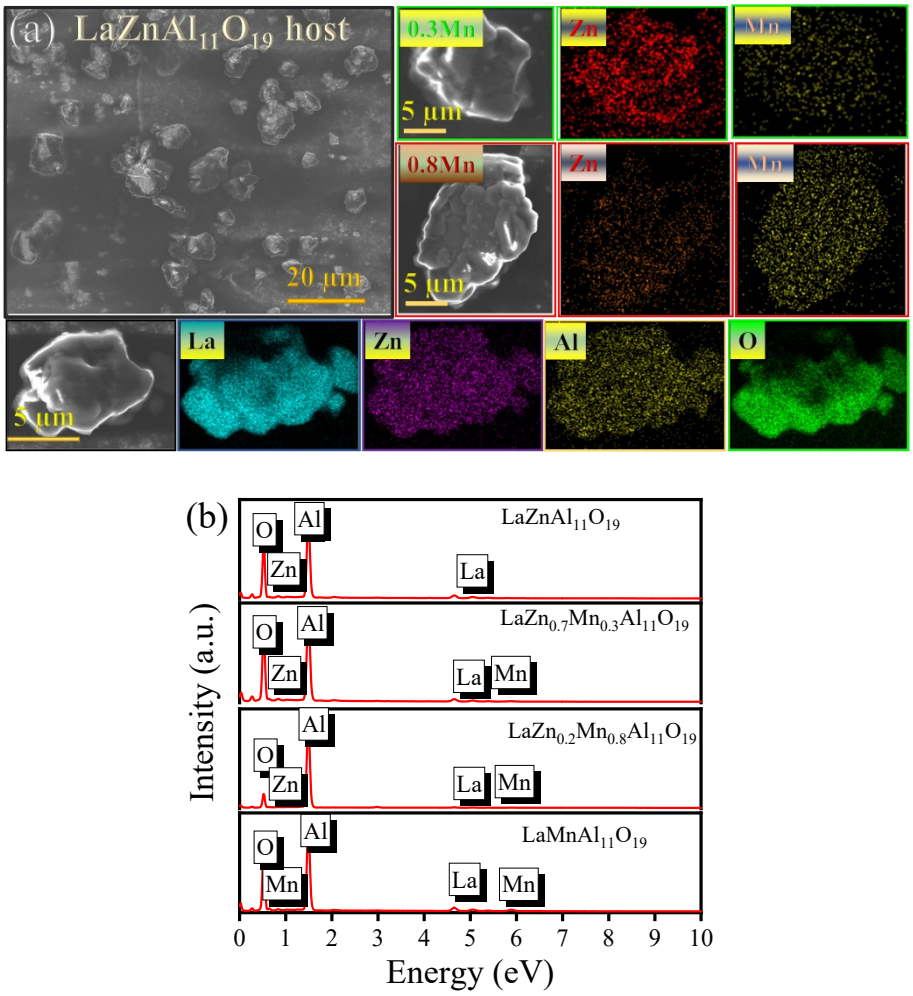

Figure S5. (a) SEM image of $LaZnAl_{11}O_{19}$ and elemental mapping of $La(Zn_{1-x}Mn_x)Al_{11}O_{19}$ (x = 0, 0.3 and 0.8). (b) EDS data and elemental contents of $LaZn_{1-x}Mn_xAl_{11}O_{19}$ with x = 0, 0.3, 0.8 and 1.

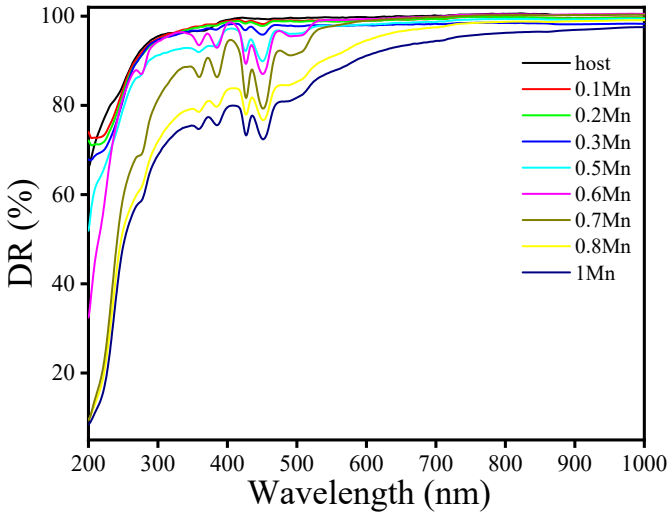

Figure S6. DR spectra of $LaZn_{1-x}Mn_xAl_{11}O_{19}$ samples.

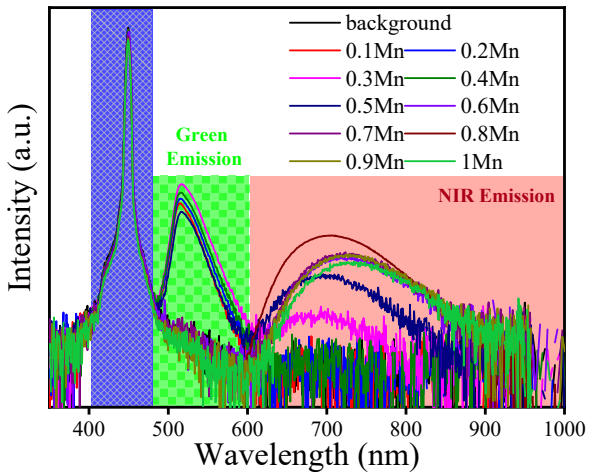

Figure S7. QE spectra and values of $LaZn_{1-x}Mn_xAl_{11}O_{19}$ with x = 0-1.

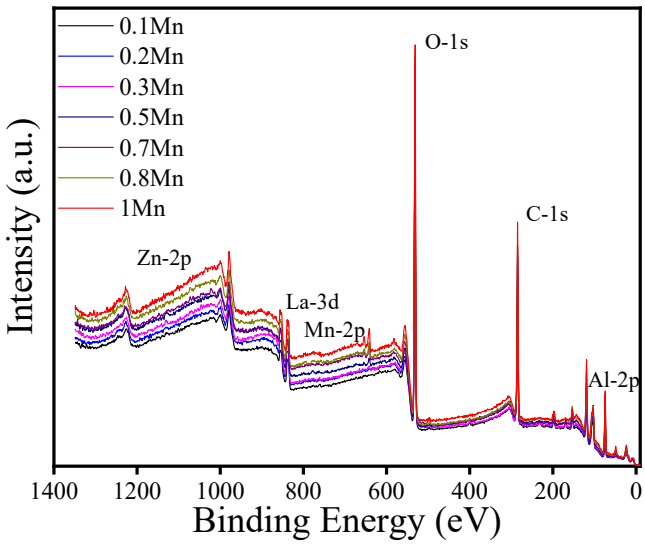

Figure S8. XPS spectra of $LaZn_{1-x}Mn_xAl_{11}O_{19}$ (x = 0-1).

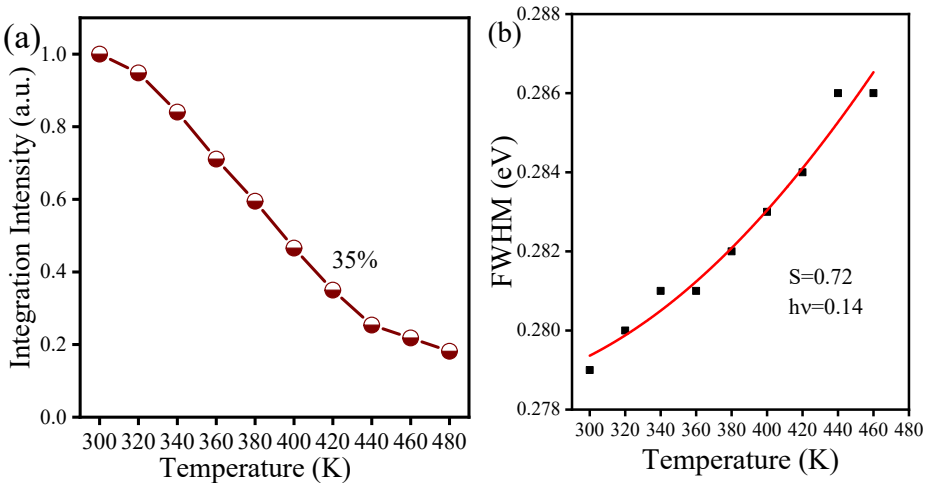

Figure S9. (a) Integrated emission intensity of $LaZn_{0.2}Mn_{0.8}Al_{11}O_{19}$ at various heating temperature, and (b) the corresponding Huang-Phys parameter.

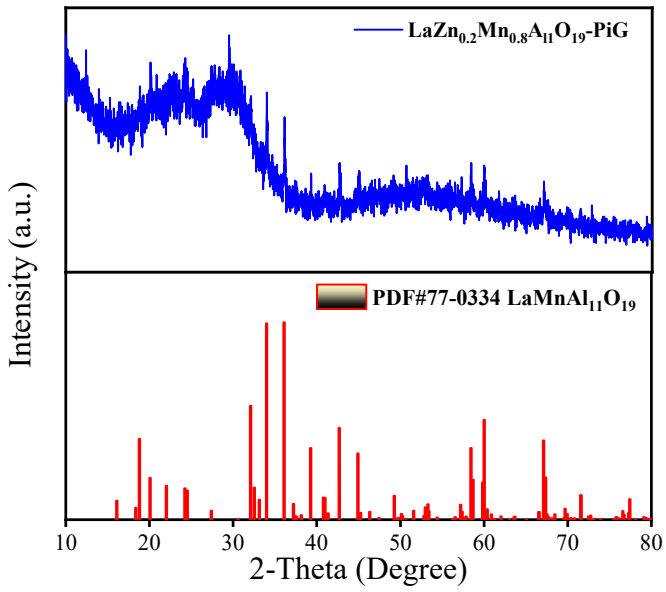

Figure S10. XRD pattern of $LaZn_{0.2}Mn_{0.8}Al_{11}O_{19}$-PiG sample

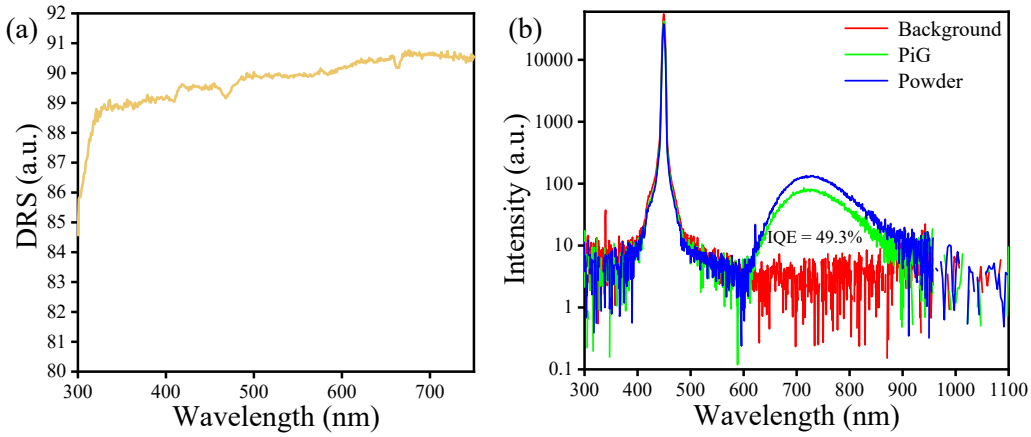

Figure S11. (a) (b) DR and QE spectra of PiG sample.

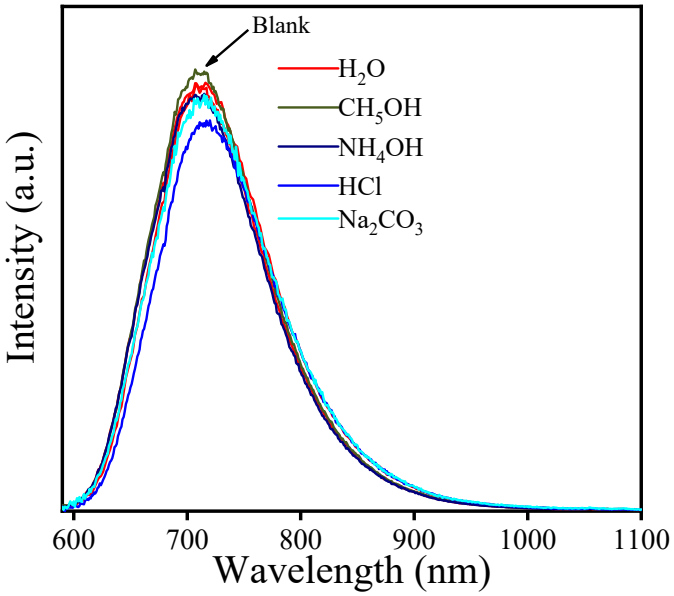

Figure S12. The emission spectra of PiG immersed in various containers.

Table S1. The refinement results of $La(Zn,Mn)Al_{11}O_{19}$

Sample	Crystallographic Parameters					Reliability Factors		
	a=b(Å)	c(Å)	V(Å^3)	α=β(°)	γ(°)	R_p(%)	R_{wp}(%)	R_{exp}(%)
x=0	5.558	19.08	589.6	90	120	7.21	9.40	6.22
x=0.2	5.565	19.08	590.9	90	120	8.92	10.38	5.89
x=0.3	5.570	19.07	591.8	90	120	5.68	7.47	4.44
x=0.4	5.574	19.08	592.5	90	120	6.33	8.69	2.83
x=0.5	5.581	19.05	593.3	90	120	9.45	11.23	7.53
x=0.6	5.584	19.07	594.9	90	120	10.42	12.65	8.05
x=0.7	5.597	19.06	597.3	90	120	11.42	14.6	4.86
x=0.8	5.599	19.07	597.8	90	120	6.00	8.13	5.60
x=1.0	5.602	19.09	599.1	90	120	13.20	14.1	8.30

Table S2. The QE value of La(Zn,Mn)$Al_{11}O_{19}$ phosphor

ratio of Zn:Mn	IQE-green part (%)	IQE-NIR part (%)	Abs
10:0	48.2	-1.6	0.053
8:2	65.4	-0.7	0.076
7:3	99.9	-1.7	0.06
6:4	57.5	3.9	0.142
5:5	28.5	12.9	0.121
4:6	0.43	28.6	0.16
3:7	0.20	36.7	0.207
2:8	0.00	55.7	0.207
1:9	0.00	21.2	0.269
10:0	0.00	16.1	0.298

Table S3. The typical doublet with 3/2 and 1/2 spin of Mn^{2+}.

Sample	$2p_{3/2}$ (eV)	$2p_{1/2}$ (eV)	Peak I-Peak II (eV)
0.1Mn	641.67	655.08	13.47
0.2Mn	642.78	654.78	12.00
0.3Mn	641.40	653.38	11.98
0.5Mn	642.58	654.48	11.90
0.7Mn	643.08	654.78	11.70
0.8Mn	642.98	654.58	11.60
0.10Mn	642.58	654.18	11.60

Table S4. The photoelectric parameters of NIR-LED

current(mA)	NIR-Output (mW)	Input (mW)	Photoelectric efficiencies(%)
50	5.6	134	4.2
100	9.5	277	3.4
150	12.4	426	2.9
200	14.7	581	2.5
250	16.7	741	2.3
300	18.5	909	2.0